Research Article

Deep Disaster-Net: A Multi-Objective Gradient-Hopping Optimized Framework with Adaptive Classifier Fusion for Post-Disaster Image Segmentation

Merdin Shamal Salih[1], Zakir Hussain Ahmed[2*] , Dilovan Asaad Zebari[3,4], Nechirvan Asaad Zebari[5], Habibollah Haron[6], Reving Masoud Abdulhakeem[7], Harish Garg[8], Ibrahim Aldayel[2]

[1] Department of Computer Science, Cihan University-Duhok, Duhok, Kurdistan Region, 42001, Iraq
[2] Department of Mathematics and Statistics, College of Science, Imam Mohammad Ibn Saud Islamic University (IMSIU), Riyadh, 11432, Saudi Arabia
[3] Department of Information Technology, Technical College of Informatics, Akre University for Applied Sciences, Akre, Kurdistan Region, 42004, Iraq
[4] Faculty of Computing and Information Technology, Sohar University, Sohar, 311, Oman
[5] Department of Information Technology, Lebanese French University, Erbil, Kurdistan Region, 44001, Iraq
[6] Faculty of Computer Science and Engineering, University of Malaysia (UNIMY), Cyberjaya, 63000, Malaysia
[7] Computer and Communication Engineering Department, Nawroz University, Duhok, Kurdistan Region, 42001, Iraq
[8] Department of Mathematics, Thapar Institute of Engineering and Technology (Deemed University), Patiala, Punjab, 147004, India
 E-mail: zaahmed@imamu.edu.sa

Abstract: Analysis of satellite images is an essential role in the response and recovery of disaster situations especially after a natural disaster like the hurricane. The conventional approaches of assessing damage heavily depend on manual examination and the antique paradigm of classification having the lexicon of limitations of being scalable, versatile and expedient. This paper presents the hybrid machine learning framework to focus on the problems of post-hurricane satellite images segmentation and classification. The solution being proposed is one which interpolates a Gradient-Hopping Hybrid Optimizer (GHHO) and a Pattern-Adaptive Classifier Fusion (PACF) mechanism. GHHO amalgamates, global exploration, and local exploitation as stochastic perturbation and local gradient descent, respectively, to maximize the optimization of segmentation parameters. At the same time, PACF will be adaptively choosing and fusing different classifiers with different feature subsets, which allows the model to react competently to the differences in land structures, atmospheric conditions, and sensor features. To improve the results further we propose a modification called Multi-Objective Gradient-Hopping Hybrid Optimizer (MO-GHHO) + PACF that involves multi-objective optimization to find improved convergence, generalization, and accuracy. The strength and versatility of both models is supported by experiments on high-resolution post-hurricane satellite datasets. The GHHO + PACF model reached the overall accuracy of 95.2% and surpassed the traditional architectures like Visual Geometry Group (VGG)-19, ResNet-50, Inception V3. Also, MO-GHHO + PACF achieves 98.2% of the land classification and 96.1% of the water body segmentation in addition to its significant increase in precision, recall, and F1 score. An ablation study also indicates the effectiveness in the individual contribution of the GHHO and PACF components in the model. The results indicate that the frameworks of GHHO + PACF and MO-GHHO + PACF have a robust, scalable, flexible application to the post-disaster analysis of satellite images and have a great potential as the decision support mechanism to any future rapid damage assessment systems.

1. Introduction

Hurricanes, typhoons, and cyclones, which are natural disasters, lead to massive and in most cases unpredictable loss on both the natural and built environment. Such damage needs to be evaluated as quickly as possible to coordinate an efficient disaster response, thus, that emergency services, humanitarian organizations and government entities could deploy the necessary resources effectively [1]. The wide extent of satellite imaging, its timely nature, and capacity to provide details about visual imaging in areas where there is no-go area or a high-risk situation makes satellite imaging an advantage in post-disaster situation [2].

Although the potential of satellite imagery is apparent, the historically used approaches to post-disaster analysis continue to be mostly manual or semi-automated and are based on human observation or structured but basic classification [3]. These methods are plagued with several failings, namely, they are computationally intensive and time-consuming, prone to error and cannot keep pace with the continuously rising volume and complexity of satellite data. A typical problem with the static classification models is the ability to generalize with other landscapes, atmospheric conditions, and imaging sensors [4]. The latest developments in machine learning, especially deep learning and evolutionary computation, have proven very promising in the automatization of analysis of satellite images. Convolutional Neural Networks (CNNs) and metaheuristic optimization algorithms have already demonstrated significant success both when it comes to extracting hierarchical features out of imagery and fine-tuning segmentation and classification models. Nevertheless, they are also subject to limitations of overfitting, data balancing sensitivity and being stuck at local minimum when optimizing [5, 6].

Recent studies have discussed the combination of aerial and satellite images to perform segmentation and classification. Arabi Aliabad et al. [7] combined the high-resolution aerial Red, Green, Blue (RGB) and Sentinel-2 images (2018-2022) to track gardens in a dry urban area and used object-oriented classifiers, namely, Support Vector Machines (SVM), Random Forest (RF), K-Nearest Neighbors (KNN) based on the Normalized Difference Vegetation Index (NDVI) and Digital Surface Model (DSM) features reaching an overall accuracy about 86.2% and the Kappa coefficient about 0.89%. Haghighi et al. [8] examined the combination of aerial imaging (30 cm resolution) with Sentinel-2 spectral indices to extract building footprints, which they trained U-Net + ResNet-34 models that had an IoU of 73.86%, F1-score of 90.57% and accuracy of 96.99%. It is these studies that recognize the benefits of integrating the fine spatial information of aerial with the spectral and contextual information of satellite imagery, and such is especially the case with small or complex urban features. Based on these bases, our proposed algorithm Pattern-Adaptive Classifier Fusion (PACF) + Multi-Objective Gradient-Hopping Hybrid Optimizer (MO-GHHO) presents a new meta-learning-based Pattern-Adaptive Classifier Fusion strategy together with MO-GHHO. In contrast to the earlier literature, which employs fixed combination of fusing strategies or works focused on single-objective training, we are dynamic in updating the weights of the classifiers based on features-specific ensembles and optimizing the accuracy and classification resistance based on varying feature distributions. This two-stage innovation improves convergence stability, overfitting, and high performance in the segmentation of water bodies and small-scale urban features in different environmental conditions.

Here we have proposed a new hybrid scheme of processing satellite images after hurricanes, and it has incorporated two important aspects in this scheme:

• Gradient-Hopping Hybrid Optimizer (GHHO): The optimizer combines the high-dimensional search ability of stochastic hopping mechanisms and the accuracy of gradient descent methods to search over multi-dimensional parameter spaces and keep out of local optima.

• PACF: Dynamic adaptation of the classification methods (patterns) to the features of input features is achieved by fusing the approaches decision trees and support vector machines adapted to each of the input features.

In contrast to the conventional deep learning structures, where a pre-defined classification pipeline is used, the PACF module reconfigures its own structure, which is an ensemble-like ensemble of patterns, to match the analysis of the

patterns. This increases the accuracy of classification and generalization of different heterogeneous input situations. How the GHHO fits into this flexibility is its ability to optimize the segmentation parameters well under different conditions. The main contributions of this study are given as:

• Our proposed MO-GHHO simultaneously maximizes both segmentation accuracy and model compactness and model computational efficiency. Such extension allows reaching a reasonable trade-off between accuracy and performance, which is essential in disaster response applications in real-time.

• PACF is proposed using meta-learning-based ensemble weighting, so the model can learn about the best fusion-based on holdout performance. This boosts the flexibility and decision-making ability of the classifier under different post-disaster scenarios.

• The hybrid MO-GHHO optimizer not only optimizes the refinement method to the local gradient descent but also allows global search by stochastic hopping, leading to a more robust convergence in the high dimensional parameter space of satellite image segmentation.

• The meta-learned weights of fusion in PACF vary dynamically in response to performance of each feature-specific classifier, ablating the ensemble to be able to better generalize to previously unseen conditions and variable atmospheric or structural conditions after a hurricane.

The final part of this article is devoted to a comprehensive literature review and provides an analysis of the strengths and weaknesses of existing models. Section 3 provides an overview of the proposed work and discusses its contributions in the field of segmentation, classification, and optimization. In section 4, the paper deals with the presentation and subsequent discussion of the results, including an ablation study that analyses the individual effects of the main components. The culmination of the research is summarized in section 5, where the authors provide a final summary and draw comprehensive conclusions from the research work.

2. Related work

The recent developments in classification of remote sensing images have seen several new models that are more accurate and efficient. SimPoolFormer is a two-stream attention-in-attention transformer with efficient capture of both spatial and spectral features [9]. Tri-Convolutional Neural Network (CNN) uses a parallel branches multi-scale 3D convolutional network to extract and combine the spectral, spatial and spectral-spatial features [10]. Non-Euclidean structures have also been popular to use the techniques of graph neural networks, which are summarized in [11], including both the traditional and deep learning techniques.

The focus of [12] is on post-hurricane damage assessment, which is an important component for emergency managers to enable effective response and resource allocation. In the past, determining the degree of damage required time-consuming and labor-intensive ground surveys, especially for buildings. The study suggests using post-hurricane satellite imagery to train image classification systems in order to increase efficiency. The authors create training, validation, and test datasets by extracting square-sized images from the satellite data at known building coordinates. Subsequently, a crowdsourcing initiative labels each photograph as either 'Flooded/Damaged' or 'Undamaged'. An existing, commonly used neural network for object categorization is compared to the performance of a CNN that is developed and trained from scratch [13]. Using satellite imagery, Ramlal et al. [14] provides a system for quickly assessing structure damage following a hurricane. The writers concentrate on tiny island republics in the Caribbean because they understand how crucial it is to provide emergency responders with fast information in the wake of disasters. They demonstrate the possibilities of remote sensing by contrasting pixel-based and object-based techniques in relation to the effects of Hurricane Ivan on Grenada in 2004. The study highlights how well the Object-Based method works with eCognition Developer Software's picture segmentation and classification features. This method considers the morphological characteristics, textural aspects, contextual information, and spectral content of image objects. Surprisingly, the Object-Based technique demonstrates its promise for quick and accurate building damage assessment by achieving above 85% classification accuracy within a three-grade damage rating scheme.

The substantial structural losses in buildings, especially because of wind-induced damage from tropical cyclones, are discussed in [15]. Using pre-and post-storm satellite pictures, the research suggests a wavelet-based change detection method for determining damage to cyclone-prone building roof systems, with a focus on the coasts of Punta Gorda prior to and following Hurricane 'Charley' in 2004. This method uses Artificial Neural Networks (ANN) and SVM for edge detection, classification, and wavelet-extracted statistical data to autonomously identify damaged buildings. Comparative studies show that wavelet-based approaches outperform traditional change detection approaches in detecting damaged buildings. This study also presents a novel Texture His wavelet approach, which was validated by manually counting damaged pixels and determining the percentage of damaged area for each building.

McCarthy et al. [16] discussed the dramatic loss of wetlands, highlighting their vulnerability to disasters such as Hurricane Irma. This study uses multispectral photography from commercial satellites to map storm damage focused on southwest Florida. This study evaluates the effectiveness of machine learning techniques (support vector machines and neural networks) and traditional decision tree approaches in distinguishing between flora that occur in wetlands and areas that do not. The decision tree approach is better at detecting healthy mangroves, while the neural network approach shows higher accuracy for degraded mangroves, but the overall accuracy is comparable. Research highlights the challenges and trade-offs associated with selecting mapping techniques for comprehensive, high-resolution assessments of damage to coastal habitats.

Kosianka et al. [17] outlines new pre-and post-storm monitoring strategy being deployed by Ursa Space Systems that leverages advanced analytics and Synthetic Aperture Radar (SAR) satellites. Ursa Space uses low-resolution SAR data to create historical change maps and uses a virtual constellation of SAR satellites to obtain a preliminary understanding of sensitive zones. This data is analyzed to identify trends and notable change events. High-resolution SAR data is used strategically using storm tracks and pre-hurricane weather forecasts to provide the basis for post-flood mapping. After a storm, data collection tracks the area and creates an aggregate data layer that represents standing water, storm damage, and land use/land cover status. Guo and Wu [18] discussed the difficulty of finding missing people or injured people in post-hurricane satellite photos, highlighting the requirement for a useful analysis technique. Based on satellite data, the study presents a stacked convolutional neural network architecture that uses classical models, such as VGG-16 and MobileNet, to identify damaged or undamaged structures in hurricane-affected areas. Remarkably, the suggested model strikes a compromise between model complexity and accuracy by outperforming VGG-16 with just six convolutional layers. In order to improve model stability and generalization, data augmentation is used. The paper emphasizes the trade-off between accuracy and model complexity, pointing out that since satellite photos aren't very detailed, using fewer layers can increase computational efficiency without sacrificing accuracy. Jiang and Friedland [19] discussed the restricted application of automated remote sensing techniques for hurricane event damage assessment, especially for low-rise structures. With an emphasis on the distinctive damage characteristics of hurricane-induced hazards, they describe a mono-temporal image classification algorithm designed to quickly and accurately separate urban debris from non-debris areas in post-event photos. In Gulfport, Mississippi, three classification strategies spectral, textural, and combination spectral textural are illustrated using National Oceanic and Atmospheric Administration (NOAA) aerial color imagery and IKONOS panchromatic satellite images following Hurricane Katrina. The findings show that by lowering misunderstanding between debris and other land cover categories, the inclusion of multivariate texture information greatly improves debris class detection. The retrieved debris border is constant across several imaging types, demonstrating the flexibility and robustness of the suggested methodology.

Kaur et al. [20] discussed the difficulties associated with hurricane-related damage assessment procedures that are cumbersome, costly, and prone to mistakes. They suggest a brand-new CNN model that makes use of satellite photos to evaluate storm damage. To expedite the provision of relief supplies to affected areas, the model focuses on identifying both damaged and undamaged buildings. The model, which is made up of two dense layers, five pooling layers, five convolutional layers, one flattening layer, one dropout layer, and one dropout layer, is trained using 23,000 128 × 128-pixel photos from the Hurricane Harvey dataset. The proposed model achieved an accuracy of 0.95 and a precision of 0.97 when the Adam optimizer was simulated on 5,750 test images using 30 epochs and a learning rate of 0.00001. Dotel et al. [21] researched the application of deep learning, specifically CNN, to disaster impact assessment using satellite imagery. Focusing on water-related disasters like floods and hurricanes, the study aims to identify impacted regions by semantically

segmenting topographical features such as roads in pre-and post-disaster satellite images. For rural landscapes with sparse topographical features, a bitemporal image classification approach is proposed to directly identify impacted regions. The method is tested on a ground truth satellite image from DigitalGlobe depicting the impacts of Hurricane Harvey, achieving an accuracy of 0.845 and an F1-Score of 0.675 in flooded road extraction. Using aerial images, Li et al. [22] tackled the problem of quickly assessing building damage following hurricanes. The authors suggest a semi supervised classification strategy in recognition of the drawbacks of supervised classification techniques, which include the requirement for many labelled samples. Three parts make up the method segmentation, Convolutional AutoEncoders (CAE) for unsupervised pretraining, and CNN for supervised fine-tuning. The learned information is transmitted to the CNN by utilizing the representation capacity of CAE. A few labelled samples are then used to tune the CNN and enhance feature discrimination. This paper uses a case study of a coastal region affected by Hurricane Sandy in 2012 to illustrate this methodology, achieving an overall accuracy of 88.3%. A comparative analysis of the above models is discussed in Table 1.

Table 1. Comparative analysis of existing models in satellite image analysis

Ref	Dataset	Method	Accuracy	Performance highlights	Challenges
[12]	Satellite imagery	CNN for building damage annotation	93%	Efficient post-hurricane assessment	Relies on labelled data availability
[14]	Satellite imagery	Rapid building damage assessment method	88%	Quick response for emergency management	May have limited accuracy in specific scenarios
[16]	Satellite imagery	Comparative analysis of satellite methods	92%	Provides insights into different monitoring methods	Resource-intensive; may require specialized knowledge
[17]	SAR imagery	Data-driven SAR monitoring	87%	Effective use of Synthetic Aperture Radar data	Limited applicability in certain regions
[18]	Satellite images	Convolutional Neural Networks	94%	Utilizes multiple CNN variants for enhanced analysis	Computational complexity may vary
[19]	Satellite + Aerial	Urban Debris Zone extraction	82%	Flexible methodology for different disaster types	Performance may vary in rural landscapes
[20]	Satellite images	CNN for Hurricane Damage detection	95%	Rapid and accurate damage assessment	Relies on labelled data availability
[21]	Satellite imagery	Deep Learning for Topographical Features	88%	Effective identification of water-related disasters	Limited applicability in sparse topography
[22]	Aerial imagery	Semi supervised CNN classification	91%	Uses both labelled and unlabelled samples for training	Initial setup may require labelled samples
[23]	Satellite imagery	Spectral Analysis	85%	Provides broad coverage	Limited accuracy in detailed damage assessment

A review of the literature provides a thorough analysis of studies conducted in the field of post-hurricane damage assessment using remote sensing and satellite imagery. Studies such as Wang et al. [23], Cao and Choe [12], and McCarthy et al. [16] investigated several approaches, including CNNs, geolocation features, and SAR-based analyses. These efforts demonstrate the importance of quickly and accurately assessing damage to allocate resources and respond effectively to emergencies. Still, there are issues such as labelled data requirements, local restrictions, and data processing complexity. The proposed study attempts to fill these gaps by using feature-specific ensemble models and hybrid optimization techniques. This method aims to improve classification accuracy while mitigating the shortcomings identified in the current study, especially under difficult conditions. The objective of the proposed model is to advance the field by providing a more reliable and adaptive hurricane damage assessment solution that improves response time and reliability.

3. Proposed method

This section described the proposed hybrid post-disaster satellite image analysis framework that has incorporated two optimized modules, which are a MO-GHHO to optimize the parameters of the segmentation and a PACF mechanism that uses meta-learning-based weighted ensemble to classify. The MO-GHHO module replaces GHHO by adding the capability to optimize several conflicting tasks simultaneously, to optimize segmentation quality, the time needed to

process the data and the compactness of the model. It makes use of a Pareto-based optimization approach that balances both global explorations using stochastic hopping with local optimization by gradient descent and guarantees sound convergence within the complex, high dimension search space.

The second module, called PACF, includes an ensemble of feature-specific classifiers and it dynamically learns the optimum fusion weights using a meta-learner. This meta-learning method also allows the system to adapt the decision strategy to the patterns observed during the validation process, which greatly increases flexibility and classification accuracy when the conditions on the ground become more diverse after the hurricane. These two elements act as a hybrid model that is effective and capable of handling high-resolution satellite images correctly, when it comes to performing segmentation operations in dynamic and changing post-disaster settings.

3.1 *Proposed MO-GHHO*

GHHO is a new optimization approach designed to solve those problems that are related to satellite image segmentation [24, 25]. Unlike the conventional methods of optimization, GHHO finds optimal high-dimensional segmentation models in a more efficient way by integrating the benefits of stochastic optimization methods along with those of gradient-based methods. GHHO employs gradient data to explore the parameter space. Moreover, its special hopping procedure provides randomness that does not allow the optimizer to obtain trapped in the local minima and can search in the solution space. GHHO is outstanding when it comes to segmenting the satellite images since it balances exploration and exploitation and effectively works with the intricate image forms and the intricacy of the large-scale patterns of land covers. Optimizers can be applied to fine-tune segmentation models because they can be reacted to the evolving features of satellite images in a flexible way and prevent inappropriate solutions. GHHO also has a significant role in the accuracy of segmentation, in that the models are able to capture more of the finer details of the satellite images and also enhance the overall quality of the results.

In addition, our MO-GHHO also optimizes both the model computational efficiency and model compactness in addition to its segmentation accuracy. It is through this form of extension that acceptable trade-off between performance and accuracy can be found which is vital when disaster response applications are being considered as the responses should be Realtime.

Initialize the parameters as θ_0, θ_1, ..., θ_n. Define the objective function to be optimized as $J(\theta)$. The slope of the objective function for each parameter is calculated according to equation (1).

$$\nabla J(\theta) = \left[\frac{\delta J}{\delta \theta_0}, \frac{\delta J}{\delta \theta_1}, \ldots\ldots, \frac{\delta J}{\delta \theta_n} \right]. \tag{1}$$

Random perturbations to the parameters are discussed in equation (2).

$$\Delta \theta i \sim U(-\varepsilon, \varepsilon), \; i = 0, 1, \ldots, n. \tag{2}$$

$U(-\varepsilon, \varepsilon)$ represent uniform distribution, each parameter using a combination of the gradient and random perturbation was updated using the equation (3).

$$\theta i \leftarrow \theta i - \alpha \nabla J(\theta i) + \beta \Delta \theta i, \; i = 0, 1, \ldots, n. \tag{3}$$

In this case, $J(\theta)$ represents the gradient descent learning rate α, and β is a hyper parameter that regulates the impact of random perturbation. By utilizing the advantages of both deterministic and stochastic optimization approaches, GHHO can efficiently explore the parameter space through the combination of gradient descent and random perturbation.

The hyper parameter β and the learning rate α are critical in determining how much gradient information and random exploration are affected in tandem. The variable $X_i(t)$ is represented as initialization of position and $V_i(t)$ represents the initialization of velocity.

$$w(t+1) = w_{\max} - \frac{t}{\max - \text{iterations}} \cdot (w_{\max} - w_{\min}), \tag{4}$$

where $w_{\max}$ and $w_{\min}$ are the maximum and minimum inertia weights, respectively. This equation (4) represents the Inertia Weight Update. The velocity update is represented in equation (5).

$$V_i(t+1) = w(t+1) \cdot V_i(t) + c_1 \cdot r_1 \cdot (P_i - X_i(t)) + c_2 \cdot r_3 \cdot (G - X_i(t)). \tag{5}$$

The position is updated as per the equation (6) and the updated personal best position is represented in equation (7). When Fitness $X_i(t+1) <$ Fitness (P_i), then the following equation (7) will be performed to update the position.

In this case, P_i (personal best position) is a best solution that has been reached to date by the i-th agent (grasshopper) in the optimization process. Every grasshopper has its own P_i, on which it can refer to regulate its movement. G (global best position) is the optimal solution of all the grasshoppers in the swarm. G is replaced by a grasshopper finding a solution with an improved fitness value than the current best in the world. Through addition of both P_i and G, the MO-GHHO algorithm balances exploration and exploitation with P_i encouraging the local search of each grasshopper across all the best experiences of the grasshopper and G steering the population towards the optimum solution in the entire world.

$$X_i(t+1) = X_i(t) + V_i(t+1) \tag{6}$$

$$P_i = X_i(t+1). \tag{7}$$

Finally, the global best position is updated as per the equation (8). r_1 and r_2 are the random numbers between 0 and 1. The boundary handling values are represented in equation (9) when Fitness $(X_i(t+1)) <$ Fitness (G). The process will be ended when $t \geq \text{max\_iterations}$ or a specified condition is met.

$$G = X_i(t+1) \tag{8}$$

The position update equation (9) is used to include a gradient descent-based position update in the Grasshopper optimization algorithm. The goal function's steepest descent is the direction that the gradient descent update seeks to travel in, and $J(\theta)$ is consistently used throughout:

$$X_i(t+1) = X_i(t) - \eta \nabla f(X_i(t)) + V_i(t+1). \tag{9}$$

Where, the gradient of the objective function with respect to the location $(X_i(t))$ is equal to $\nabla f(X_i(t))$. The gradient descent update's step size is determined by the learning rate, represented as η. This formula combines the gradient descent update with the movement caused by the current velocity, $V_i(t+1)$. The gradient descent term $\eta \nabla f(X_i(t))$ modifies the position according to the local knowledge of the slope of the objective function. When the Grasshopper Optimisation Algorithm takes this into account, the entire position update is represented in equation (10).

Equations (6)-(8) carry out the usual position and velocity update founded on the present velocity of the swarm and the impact of the personal and global best positions. This update causes every grasshopper to go towards any promising regions of the search space. Once this movement has been done, equation (9) is used as the next refinement step which takes into consideration the gradient descent. The gradient-based correction optimizes the newly updated position as of equation (6) by taking advantage of local slope information of the objective function. This two-step exploration strategy based on update velocity, and then gradient exploitation enables MO-GHHO to balance between global exploration and local convergence and is more accurate and stable in convergence than either update method alone.

$$X_i(t+1) = X_i(t) - \eta \nabla f(X_i(t)) + V_i(t+1). \tag{10}$$

Equations (9) and (10) are two different similar updates in MO-GHHO. Equation (9) runs a gradient-based refinement by modifying the position of each grasshopper as a result of using the local gradient of the objective function coupled with maintaining its current velocity. Equation (10) is a composite model of the position change; it is a combination of the regular swarm movement equations (6)-(8) and the gradient-based correction equation (9). This two-step algorithm trades off exploration of global forces of swarm dynamics with exploitation of local forces of gradient descent, enhancing stability of convergence and accuracy of optimization.

With this adjustment, the position update now includes a gradient-based component, which can improve the algorithm's capacity to explore the search space more efficiently, particularly when gradient information is relevant and available for the optimization objective. It is imperative to modify the learning rate (η) to maintain equilibrium between the global and individual optimal information supplied by the swarm and the influence of the gradient descent update. As well as optimizing the refinement method to the local gradient descent, the hybrid MO-GHHO optimizer can search in global mode as suggested by stochastic hopping to give a more robust convergence in the high-dimensional parameter space of satellite image segmentation.
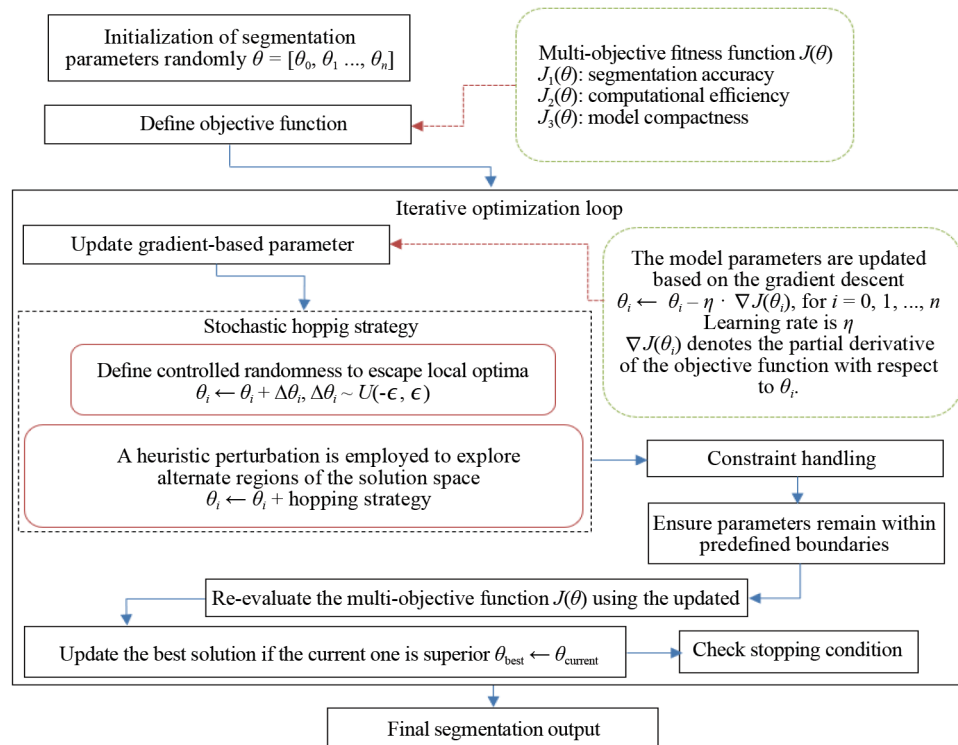

Figure 1. Proposed MO-GHHO for satellite image segmentation

The satellite image segmentation on data of high-dimension and with complicated structure would be an issue and this has been solved by use of the MO-GHHO which has been introduced. MO-GHHO offers a flexible method of exploring heterogeneous and multimodal search spaces with the ability to combine a heuristic search and gradient-based optimization. The heuristic search allows global search and eliminates the risk of the algorithm conversion towards local optimum. The gradient descent part of the algorithm is used to improve on local segmentation boundaries, and it finds small details of satellite images. The ability to work with large amounts of data, and tolerance to noise makes MO-GHHO a potential way to perform context-aware and autonomous segmentation, which will allow improving the distinctiveness of land cover boundaries in satellite data. Figure 1 contains the specific flow of works of the suggested model.
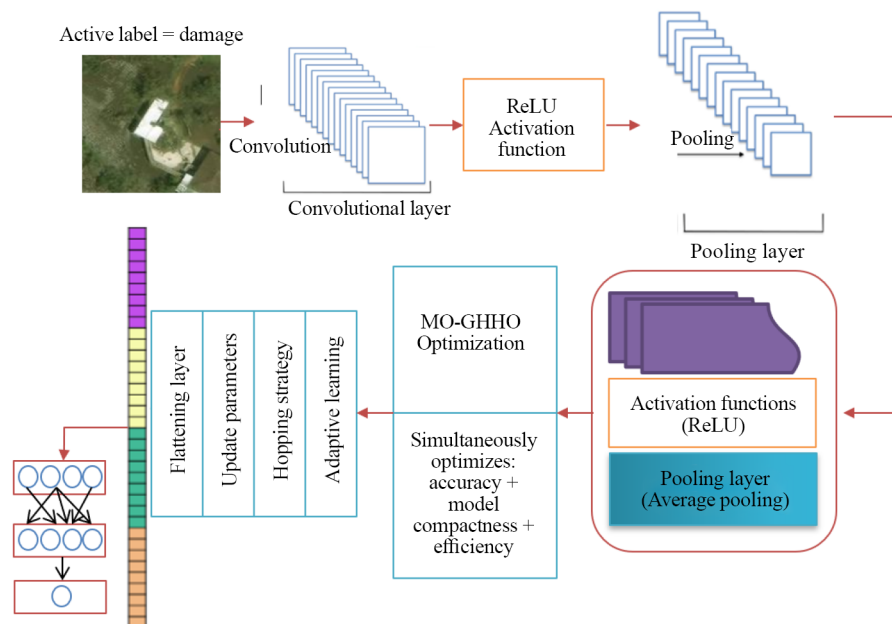

Figure 2. An architecture of regularized CNN with MO-GHHO

The input image is processed using convolutional layers and hierarchical information is captured. Such regularization methods as dropout are then used to avoid overfitting. The MO-GHHO improves the CNN on four fronts: it optimizes the learning rates during the training process, making learning dynamic and adding hopping techniques, which enables the exploration of the parameter space efficiently and convergence. This architecture combines convolutional layers with MO-GHHO as a means of placing special focus on feature extraction and on adaptive optimization, a fact that leads to a robust, properly regularized CNN with improved performance in a diverse number of image-based applications. The MO-GHHO operational flow starts with initialization segmentation parameter (randomly or heuristically), an iterative process of global search by the means of heuristic hopping and local search by gradient descent (See Figure 2). To measure the quality of segmentation an objective function is considered at every step. This process of optimization is repeated till convergence, or a stopping rule is satisfied. Optimizing in this way on a phase-to-phase basis enables the MO-GHHO to dynamically trade off exploration and exploitation in parameters space, resulting in greater segmentation accuracy.

Additionally, PACF is also implemented in the suggested framework with the help of meta-learning-based ensemble weighting. This enables the model to learn optimal fusion strategy based on holdout performance hence increasing flexibility and the decision-making capacity of the classifier under various post disaster situations. The ensemble weights of fusion are meta-learned to dynamically vary depending on how each feature-specific classifier performs and results in better generalization to unknown conditions and variable atmospheric or structural conditions after a hurricane, ablating the ensemble.

3.2 *Proposed PACF with meta-learning and feature-specific tree-SVM ensemble*

As a component of the PACF framework, the Feature-Specific Tree-SVM Ensemble is a unique technique that improves satellite image classification accuracy and adaptability [26]. Decision trees and Support Vector Machines (SVMs) that are customized to features in the satellite data are included in this ensemble method. Because each classifier in the ensemble focuses on identifying unique traits, the total categorization is more accurate and nuanced. The model can capture intricate patterns because to the usage of decision trees, and SVMs provide robustness and generalization abilities [27, 28].

The flexibility brought about by the PACF idea makes this ensemble technique very successful in managing a variety of landscapes, atmospheric conditions, and sensor specifications. Through the customization of classification approaches to feature sets, the Feature-Specific Tree-SVM Ensemble exhibits enhanced robustness and precision in many scenarios (See Figure 3). This approach performs exceptionally well in the finely detailed classification of complex patterns found in satellite data, which adds to the PACF framework's overall effectiveness in tackling the difficulties associated with satellite image analysis. The following equations from (11) to (19) specify the pattern specific classifier.

Further to improve the flexibility, we suggest a meta-learning-based ensemble weighting scheme in PACF. This mechanism enables the model to learn how to re-optimize these weights of fusion conduct based on the holdout measures of performance, making it dynamically adaptive to new scenarios after a disaster has occurred. This is a learning-style approach based on an ensemble, unlike the fixed weighting method; it gives a direct performance-related fusion strategy, enhancing the combination capabilities of the ensemble in diverse atmospheric and structural conditions. Besides, meta-learned fusion weights adapt dynamically to the variance performance of individual feature-specific classifiers. This structure allows the ensemble to be able to give more credible classifiers according to the situation at hand essentially raising generalization to conditions that it has never encountered before. This form of flexibility is imperative in applications such as post-hurricane damage assessment that become highly variable depending on the environment.

$$T_i(\mathrm{X}) = \sum_{j=1}^{j_i} w_{ij} \cdot 1_{\left\{X \in R_{ij}\right\}}. \tag{11}$$

The result of a decision tree unique to feature i in the Feature-Specific Tree-SVM Ensemble is represented by equation (11). By aggregating weighted predictions based on whether the input X falls inside the areas indicated by the tree's splits, it determines the cumulative contribution of each leaf in the tree.

$$f_i(X) = \sum_{k=1}^{N_i} \alpha_{ik} \cdot K(X, X_k) + b_i. \tag{12}$$

The output of the SVM model for features i in the Feature-Specific Tree-SVM Ensemble is represented by equation (12). The decision function $f_i(X)$ is calculated by adding up the weighted contributions of the support vectors X_k using coefficients α_{ik} and using a kernel function $K(X, X_k)$, along with an extra bias term b_i. The decision-making process of the SVM for feature i is encapsulated in this equation, which highlights the impact of pertinent support vectors on the ultimate prediction for the input X.

$$y_i(X) = \frac{\sum_{m=1}^{M} w_{mi} + C_m(X)}{\sum_{m=1}^{M} w_{mi}}. \tag{13}$$

The output $y_i(X)$ for feature i in the proposed PACF is defined by equation (13). It is an example of the dynamic fusion technique, merging the outputs of several classifiers $C_m(X)$ that are particular to feature i. To provide a normalized and adaptive fusion process, the weighted sum of each classifier's outputs is divided by the total of the adaptive weights w_{mi}. The heart of the PACF's dynamic combination of classifier outputs based on detected patterns is encapsulated in this equation, wherein weights are adjusted based on the relative performance and significance of each classifier.

$$w_m^{(t+1)} = w_m^t + \text{learning}_{\text{rate}} \cdot \frac{\partial \text{ performance } C_m}{\partial w_{mi}}. \tag{14}$$

The update rule for the classifiers in the Proposed PACF is represented by equation (14) for the adaptive weights $w_m^{(t+1)}$. It illustrates the iterative learning process in which the gradient of the relevant classifier's performance C_m and the learning rate are used to update each weight.

$$\text{Pattern}_{\text{Analysis}(X)} = \text{Entropy}_{(X)}. \tag{15}$$

In PACF, the pattern complexity is computed by computing the entropy of the input X in equation (15). The measure informs the adaptive weighting mechanism, which shows the features that have more discriminative information.

$$w_{mi} = \text{Adaptive}_{\text{Weight}\left(X, \text{ Pattern}_{\text{Analysis}(X)}\right)} \tag{16}$$

$$Y(X) = \sum_{i=1}^{F} w_i y_i(X). \tag{17}$$

The adaptive weight w_{mi} (adaptive weight) for a particular feature i in the Proposed PACF is calculated using equation (16). The adaptive function, represented as $\text{Adaptive}_{\text{Weight}\left(X, \text{ Pattern}_{\text{Analysis}(X)}\right)}$, is used in this process. It dynamically modifies the weight in accordance with the input data (X) and the associated pattern analysis. The overall decision fusion $Y(X) = f(X)$ in PACF is defined by equation (17). The fused output is produced by adding the contributions from each feature $y_i(X) = f_i(X)$ multiplied by their specific weight $y_i(X)$. The weights in this equation show how PACF aggregates data from several features to arrive at a final classification conclusion. Each feature in the ensemble is represented by its respective effect.

$$\text{Final decision } (Y(X)) = \begin{cases} 1, & \text{if } Y(X) > \text{ Threshold} \\ 0, & \text{otherwise} \end{cases}. \tag{18}$$

The final choice in the proposed PACF, indicated as $Y(X)$, is given by equation (18). It makes use of a thresholding technique, in which the output is set to 1 in the event that $Y(X)$ over a predetermined threshold and to 0 in all other cases. This stage contributes to the PACF ensemble's final classification result by converting the continuous fused output into a binary decision.

$$K(X, X_k) = exp(-2\sigma^2 \|X - X_k\|^2). \tag{19}$$

The Radial Basis Function (RBF) kernel, $K(X, X_k)$, is defined by equation (19). This kernel is utilized in the SVM model of the Feature-Specific Tree-SVM Ensemble. The similarity between input data X and a support vector k is computed using the kernel function. It utilizes the exponential term normalized by the kernel width parameter $2\sigma^2$ and with a negative squared Euclidean distance. To capture complicated correlations and non-linearities in the input data, SVMs frequently employ the RBF kernel.

$$\text{Split}_{\text{Criterion}} = \text{InformationGain}_{(Rij)} \tag{20}$$

The split criterion of the decision tree represented by equation (20) is based on information gain that is used to measure the homogeneity of the data of region Rij. This guarantees the best splits in learning which enhances the tree structure and classification accuracy.
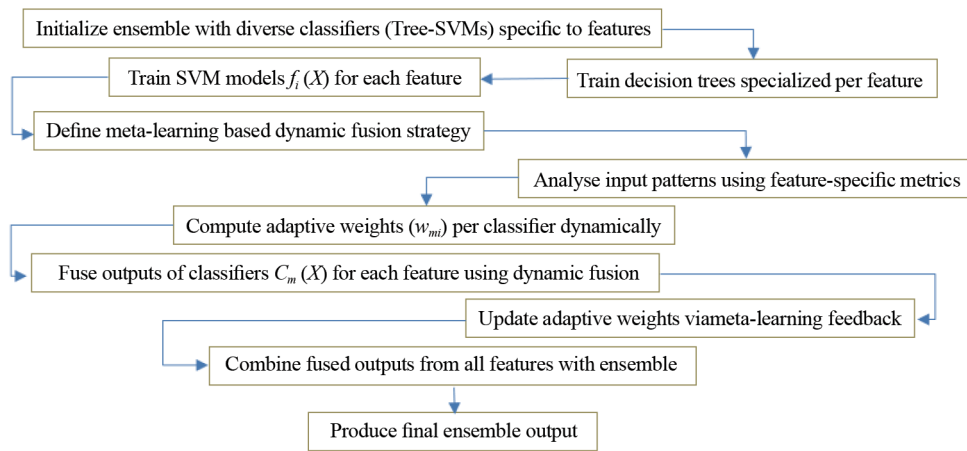

Figure 3. Working flow of the proposed PACF

PACF can be further enhanced in combination with our presented MO-GHHO. The MO-GHHO is a multi-objective algorithm that trades off all of these three things simultaneously. MO-GHHO allows to trade-off between performance and precision, thereby allowing PACF to be utilized on real-time disaster response environments, where performance speed and accuracy are both crucial. MO-GHHO uses both local gradient refinement and global stochastic hopping and thus, it is very suitable in exploring the high-dimensional parameter space associated with the satellite image segmentation models.

3.3 *Proposed GHHO-PACF model*

The proposed GHHO-PACF model combines the functionality of MO-GHHO and PACF model to create an effective and accurate classification system. The ensemble classifier and optimizer parameters are first initialized with each solution in a population having a position, a velocity, and a personal best with the global best being calculated across all solutions.

The input samples are analyzed using pattern analysis to retrieve informative features during the training phase and the adaptive weighting of the classifiers are guided by the informative features. The PACF parameters are also updated with a hybrid rule of gradient descent and random perturbations which makes the model take advantage of both deterministic and stochastic optimization. At the same time, the MO-GHHO algorithm changes the positions and velocities of the population according to personal and global bests, which balances the exploration and exploitation of the search space. Pattern analysis is applied to calculate the adaptive weights of the ensemble classifier to improve the capacity of the classifier to concentrate on the most effective features.

The dynamic fusion mechanism of PACF is used to produce outputs in the validation phase which are measured to determine performance metrics. The optimizer parameters are then adjusted using these metrics in a multi-objective feedback loop which is aimed at assuring that the algorithm keeps on improving convergence, accuracy and robustness. The proposed framework is highly effective and flexible, combining global exploration by using MO-GHHO with local exploitation by using gradient-based updates in PACF, which are effective in providing the most suitable classification model in the most challenging situations of real-time post-disaster analysis.

Algorithm 1 Proposed MO-GHHO-PACF

Input: Training data T_a, T_b

Validation data V_a, V_b

Ensemble classifier $PACF_{EC}$

Optimizer parameters $GHHO_{OP}$ [α, β, η, c_1, c_2, w_{max}, w_{min}, max_iter]

1. **Initialize**

a. Initialize $PACF_{EC}$

b. Initialize $GHHO_{OP}$

    For each solution i in population:

        Initialize position $X_i(0)$, velocity $V_i(0)$

        Set local best $P_i \leftarrow X_i(0)$

Set global best $G \leftarrow$ Best of P_i

2. **For** $t = 1$ **to** max_iter **do:**

A. Training Phase:

    For each (x, y) **in** (X_{tr}, y_{tr}) **do:**

        $pa_{res} \leftarrow$ PatternAnalysis(x)

        $\nabla J \leftarrow$ Compute Gradient$(PACF_{C, x, y})$

    $\Delta\theta \leftarrow$ RandomNoiseUniform $(-\varepsilon, \varepsilon)$

    // Hybrid Update Rule

$\theta \leftarrow \theta - \alpha \times \nabla J + \beta \times \Delta\theta$

    // MO-GHHO Update

$w_t \leftarrow w_{max} - (t/\text{max\_iter}) \times (w_{max} - w_{min})$

$r_1, r_2 \leftarrow$ Random$(0, 1)$

$V_i(t+1) \leftarrow w_t \times V_i(t) + c_1 \times r_1 \times (P_i - X_i(t)) + c_2 \times r_2 \times (G - X_i(t))$

$X_i(t+1) \leftarrow X_i(t) - \eta \times \nabla f(X_i(t)) + V_i(t+1)$

    // Update personal and global bests

    If Fitness $(X_i(t+1)) <$ Fitness (P_i) **then:**

        $P_i \leftarrow X_i(t+1)$

    If Fitness $(X_i(t+1)) <$ Fitness (G) **then:**

        $G \leftarrow X_i(t+1)$

        $a_w \leftarrow$ AdaptiveWeight (pa_{res})

        $PACF_{EC} \leftarrow$ UpdateEnsemble $(PACF_{EC}, x, y, a_w)$

B. Validation Phase:

    For each (x_v, y_v) **in** (X_{val}, y_{val}) **do:**

        $df_{res} \leftarrow$ PACF_DynamicFusion$(PACF_{EC}, x_v)$

        $v_{metric} \leftarrow$ Evaluate(df_{res}, y_v)

C. Update $GHHO_{OP}$

    Adjust α, β, η based on v_{metric} (multi-objective feedback).

3.4 *Return optimized $PACF_{EC}$*

MO_GHHO_PACF is a crossbreed smart learning component that is applied to streamline ensemble classification system. It is a combination of three major elements, such as dynamic pattern analysis PACF model, and MO-GHHO

approach. The algorithm starts its run with the initialization of a population of possible solutions and the ensemble classifier. Each sample of the inputs undergoes a pattern analysis stage which enables the algorithm to determine the structural or statistical properties and therefore the algorithm can produce adaptive learning weights depending on the particular data sample. These are weights used in the training of the PACF classifier ensemble dynamic which adjust its parameters in accordance to the nature of individual samples.

At the same time, when using globally and locally in MO-GHHO optimizer, the search is performed globally and locally. It improves the standard GHHO by complementing gradient-based updates on stochastic noise to improve search space exploration and exploitation. Both the dynamic rules of GHHO as well as the gradient information are used to update the solution vectors, and this gives faster convergence and better accuracy. During training, the algorithm keeps record of personal best and global best solutions using the multi-objective fitness criterion and the validation measures such as the accuracy, precision and F1-score. During the validation stage the decisions made by the ensemble will be merged through the PACF dynamic fusion mechanism which chooses the optimal prediction strategy by adapting on current performance. The parameters of the optimizer are also optimized based on the feedback of the validation results and improvement is always done.

In general, MO-GHHO-PACF provides considerably strong, adaptive, and high confident classification based on context-aware learning, dynamic fusion, and multi-objective optimization. It is especially efficient in more complicated, imbalanced, or noisy data, including biomedical diagnosis, fault detection, and time-series classification.
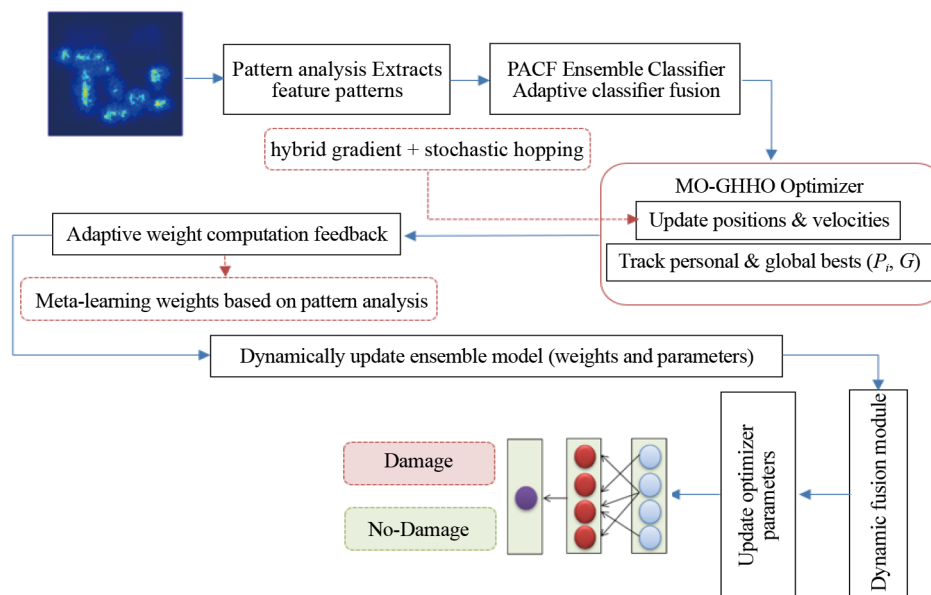

Figure 4. A network architecture of proposed MO-GHHO-PACF optimizer

Figure 4 shows the architecture of the proposed GHHO-PACF that is specific to accomplish the binary classification of satellite imagery into the damage and no damage classifications. The structure combines the MO-GHHO optimizer and the PACF ensemble to train the classifier juxtaposition in a supple manner with both the weights and excellent arrangement parameters. The MO-GHHO component is a hybrid optimization scheme that aims at striking a balance between three important goals such as, maximizing segmentation accuracy; minimizing model complexity; and even maximizing the efficient use of computer power. Such a multi-objective modelling is especially valuable in the time-sensitive applications like disaster response, where the requirement is to have real-time analysis that is light and precise.

By contrast to conventional optimizers, the proposed MO-GHHO integrates local gradient descent with stochastic hopping to produce robust convergence in high dimensional spaces of parameters. The added feature of a global search

process helps the optimizer to jump out of local optima into a wider set of better parameter configurations of the model. At the same time, PACF mechanism uses meta-learning approach to weighting the ensemble to choose the best strategy of classifier fusion. Integrating holdout performance allows the model to adaptively tune the degree of the weight on each base classifier thereby enhancing its flexibility when exposed to different post-disaster. Moreover, the pattern-adaptive and performance-sensitive fusion weights allow the system to be responsibly to structural variability and change of atmosphere in satellite images. The result of the combined approach is a robust and scalable classification pipeline that might generalize to unseen scenarios. GHHO-PACF architecture as such, presents a solid decision-making mechanism that is viable to implement into practice towards an actual disaster-assessment scenario.

4. Results and discussion
4.1 *Datasets*

The PostHurricane Satellite Imagery Dataset, featured on Kaggle and last updated three years ago, contains the total amount of 15,800 RBG satellite image patches, 128 × 128 in resolution, taken over the Greater Houston region in the wake of Hurricane Harvey (August 2017). The image data is further tidied into three sets of 10,000, 2,000 and 3,800 images to train, validate and test respectively. The signs of structural damage are marked as binary labels, and each image can be classified as having the damage or have no damage.

The Water Bodies Segmentation Dataset provided by Prasad Meesala in his Kaggle notebook is a collection of 2,841 RGB satellite images to which a binary mask is applied to segment the water bodies semantically. In such masks, the water zones are tagged with foreground (white, pixel value 255) and non-water zones with background (black, pixel value 0). All the images are of the same size and have been prepared in a standard form to be used in remote sensing analysis on pixel-to-pixel basis. Even though official split between training, validation and testing is not given in the dataset, 1,989 images are given when to train, 426 when to validate and 426 when to test. The data represents a clean and balance test platform, to test segmentation models on the clear definition of water bodies, in diverse landscapes and environmental situations.

Another data used in this research is satellite image data which has been used to carry out land cover classification tasks. It has 5,631 RGB images, all 64 × 64 pixels, spread over four semantic categories (buildings, roads, vegetation and water bodies). The dataset is sorted into 3,941 training images, 564 validation images and 1,126 testing images. The labelling of each image is done in supervised learning and it supports multi-class classification. The dataset offers the concise, yet varied view of the land cover types at the surface level, which simplifies the analysis of the lightweight deep learning models and optimization frameworks, such as MO-GHHO with PACF suggested by the research.

4.2 *Result and analysis*

The post-hurricane data in this work is comprised of a set of high-resolution satellite images which were captured after hurricanes. The dataset represents a great variety of geographical localities subjected to hurricanes such as suburban, urban and rural regions. The photographs also cover diverse topographies such as interiors, coastal areas, as well as urban centres full of people. All of the photographs show the aftermath of the hurricane on the landscape, the infrastructures, nature, and structures. To provide the appropriate information on the extent of the damage to buildings and other constructions, the dataset has been annotated. The annotation is used to define the status of a particular structure or region as being Undamaged or Flooded/Damaged. Besides, there is the addition of geolocation elements which enhance the contextual information in the dataset. The dataset considers the time aspect, reported photos captured at different times since the occurrence of the storms and indicate the change in damage and recovery.

The hyperparameters of all models were optimized with the validation set that it could perform optimally. In deep learning models such as ResNet-50, VGG-19, Inception V3, MobileNet, DenseNet, such hyperparameters as learning rate, batch size, number of epochs, and optimizers Adam were varied in order to obtain the highest convergence. Each model was also optimized with architecture-specific parameters like number of convolutional layers, number of filters and size of their kernel. In the proposed MO-GHHO + PACF hybrid model, the hyperparameters were also optimized by applying

the PACF optimization framework that improves the training convergence and general accuracy of classification. The process of hyperparameter tuning guarantees that every model is trained on the best possible settings, and it is possible to have a fair and reliable comparison between different models.
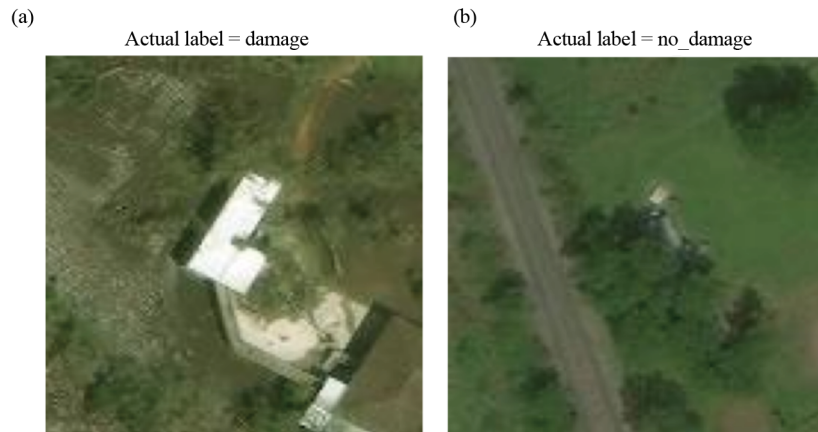
(a)
Actual label = damage

(b)
Actual label = no_damage

Figure 5. Sample dataset collection with damage and no damage label

The training set will include 10,000 images, and it will be classified into two different classes. The test sample is composed of 3,800 images as well classified under the same two classes. These data are necessary to train and test machine learning models, in other words, train them to differentiate between the two classes based on the given pictures as demonstrated in Figure 5 [18].

4.3 *Model performance analysis using NumPy*

Optimized CNN model, Resnet 50, VGG19 and InceptionV3 NumPy array allow numerical manipulation and analysis of the image data with the help of the capabilities of the NumPy library as presented in Figure 6. The NumPy array that was created has a shape of (128, 128 and 3).
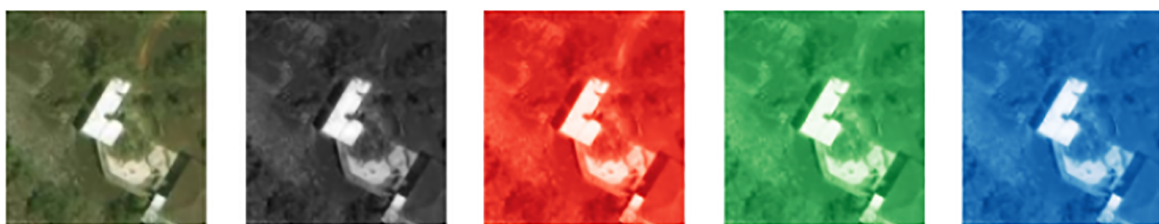

Figure 6. Image into Numpy array conversion

Subset regularized CNN architecture is represented in Table 2 and starts with a max-pooling layer maxpooling2d3 and two convolutional layers conv2d6 and conv2d7. The network then flattens the output and passes it through three dense layers dense3, dense4 and dense5 to perform classification and extract features. The model contains 127,021,985 total parameters and all of them can be trained. It is important to ensure that the model will not over fit the training data due to its size and the possibility of the model consuming a lot of computer resources during the training phase. The model architecture refers to a complex and profound neural network that can learn complex patterns.

Table 2. Subset (Regularized CNN) model summary

Layer (type)	Output shape	Param #
conv2d_6 (Conv2D)	(None, 126, 126, 32)	896
conv2d_7 (Conv2D)	(None, 124, 124, 32)	9,248
max_pooling2d_3 (MaxPooling2D)	(None, 62, 62, 32)	0
flatten_1 (Flatten)	(None, 123,008)	0
dense_3 (Dense)	(None, 1,024)	125,961,216
dense_4 (Dense)	(None, 1,024)	1,049,600
dense_5 (Dense)	(None, 1)	1,025

As demonstrated in Figure 7a, the accuracy metrics of the regularized CNN model are presented. The rate at which the instances in the training data have been correctly categorized is represented as training accuracy, and is reported to be 89%. The accuracy in the testing-data is reported simultaneously at 87%, which is the performance of the model on never-before-seen data in the testing set. These accuracy values indicate the ability of the model to learn using the training data and generalize to new unknown data; when the difference between training and test accuracy is small, the model is successful in generalization, but not by overfitting.
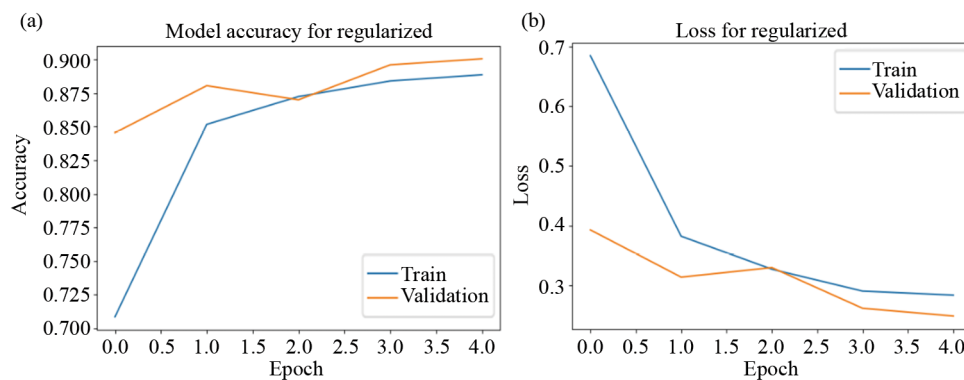

Figure 7. (a) Accuracy for regularized CNN model, (b) Loss of regularized CNN model

Figure 7b presents the loss values of the regularized CNN model. The testing loss of the model is reported as 0.3 and the training loss of the model is reported as 0.4, which is an average loss on the training dataset. These loss values indicate the extent to which the model minimizes the errors during the training and testing phase. Reduced values of losses usually show improved convergence and performance, and are used to show the extent to which the model captures and extrapolates patterns in the data. The close relationship between training and testing losses indicates that the regularization strategies used on the CNN have prevented overfitting, which has improved the generalization performance of the model.

Figure 8 visualizes the feature maps produced by regularized CNN model which would give a representation of internal activations created as a response to the input data representation. The feature maps are highly crucial in the decoding of the feature extraction hierarchy in the various locations of the network that denote selective activations of distinct layers of filters or neurons. The initial convolutional layers could contain maps containing such features as edges, textures and basic forms. The deeper the network, the more intricate the feature maps representing a more abstract component will change to represent a better semantic information that will matter to the classification or segmentation. The CNN can be improved to perform better on generalization through regularization techniques such as, dropout, weight decay or batch normalization, which can help avoid overfitting. Such techniques influence the form and frequency of output feature maps by the limitations of sparsity or constancy of learnt features. Therefore, the feature maps are not

only used to demonstrate the spatial and semantic sensitivity of the network but also used to show the strength and the discriminativeness of features being learnt due to the regularization strategy followed. In these visualizations, the researchers will be able to have helpful information about how the decision-making process of the CNN works and how the features learned about the relevant data in the different layers would be useful.
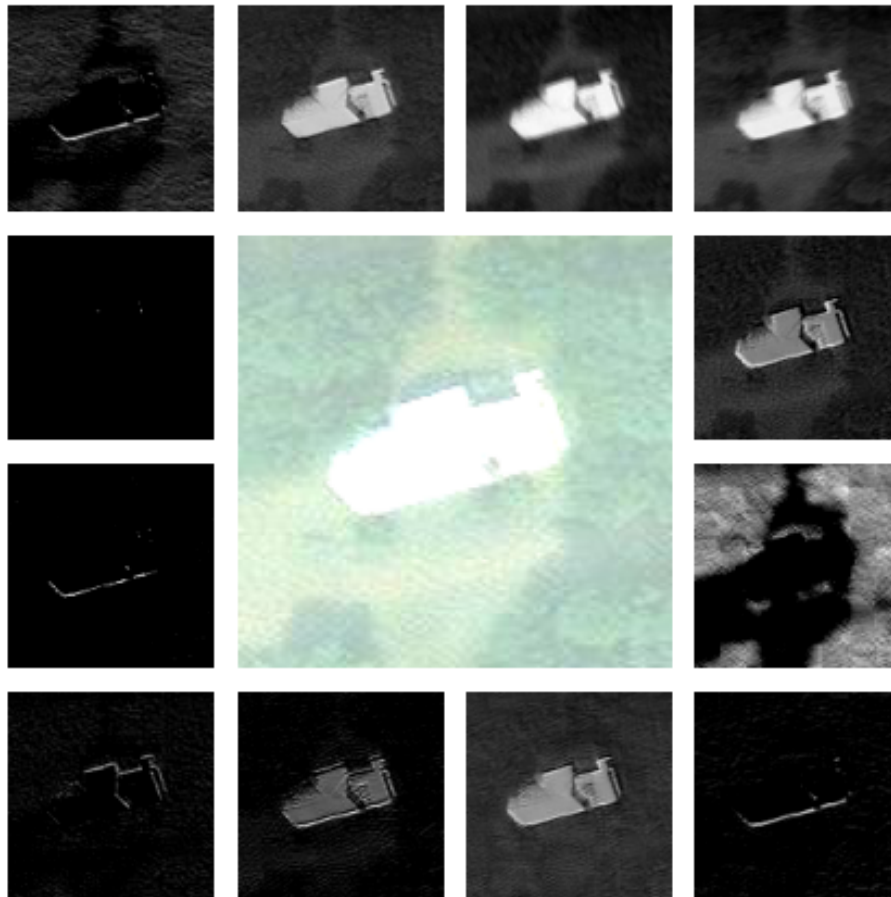

Figure 8. Feature map of regularized CNN model

Figure 9 displays the saliency maps of some of the validation images which are most likely generated in the environment of a neural network, a CNN specifically. Saliency maps are among the best instruments of interpretability as they provide an understanding of what region of input image affects most the predictions of models. They are estimated as gradient of the output score on the output classes to the pixels as the inputs, thereby, indicating what areas the network believes to be the most important in a particular decision. It is based on this that the brighter parts in the saliency maps represent parts that have experienced high gradient magnitude thus meaning that features or spatial ground that has a significant influence in the outcome of a significant model. The events occurring in these regions of interest tell us of the parts in the picture that are important in generating discriminatory cases on classes therefore providing us with a clue on how CNN brain operates. Such analysis of these maps of different samples enables investigators to assess to what degree a model is concerned with semantically significant regions without bias or whether it is interested in truly relevant features as opposed to irrelevant and ad hoc facts. This analysis is particularly significant in those fields when a certain level of transparency and trust of a model is required, such as medical diagnosis, remote sensing, and autonomous infrastructure.
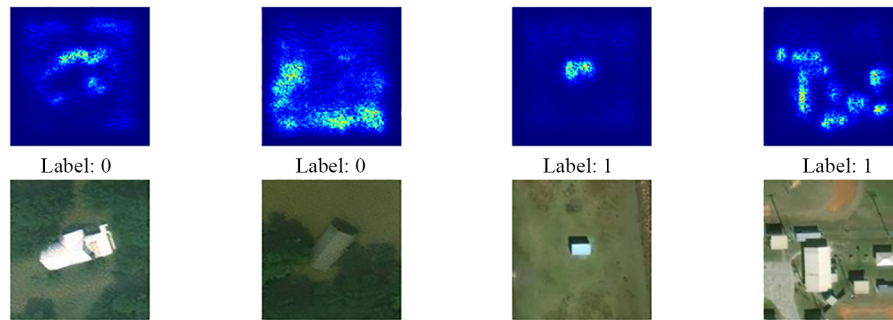
Figure 9. Saliency maps for various validation images

ResNet-50 has a deep neural network architecture of 50 layers. In the specified case, the model will not be trained on the last 30 layers because of the resource constraints or the computational efficiency. This method is known as transfer learning and the pre-trained layers are left untouched and only part of the network is retrained to work on a specific task or dataset. Based on the previously stored information in the preceding levels, the model can utilize it and adapt to the requirements of the current assignment by skipping the training of the last thirty layers.
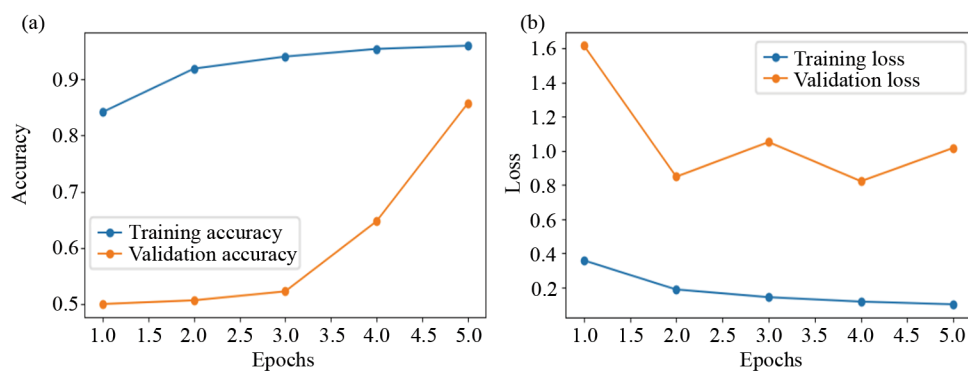

Figure 10. (a) Training and validation accuracy of ResNet-50, (b) Training and validation loss of ResNet-50

Figure 10a represents the training and validation accuracy curves of a ResNet-50 model over multiple epochs. The number of epochs is reflected on the *x*-axis and the level of accuracy in the open questions is indicated in the *y*-axis. The validation accuracy 92% and 84.2% respectively indicates the effectiveness of the model to new data, and the plot provides the view of how the performance was improved during training. Figure 10b represents training and validation loss 1% and 0.2% respectively curves of ResNet-50 model at different epochs. The training epochs are indicated on the *x*-axis whereas the loss values are indicated on the *y*-axis. The model has the ability to converge and generalise, which is illuminated by the plot.

Table 3. Accuracy and loss of training and validation data of the model

Epoch	Training loss	Training accuracy	Validation loss	Validation accuracy
1	0.3578	0.8421	1.6157	0.5005
2	0.1875	0.9191	0.8478	0.5070
3	0.1426	0.9405	1.0508	0.5230
4	0.1167	0.9541	0.8214	0.6475
5	0.1008	0.9598	1.0164	0.8570

Table 3 provides a detailed overview of the performance of the model in the five epochs of training and validation. The convergence and model learning also improves as the training loss decreases to 0.1008 when the training loss is reduced by 0.3578. At the same time, the accuracy of training steadily rises and reaches 95.98% in the final epoch. The results of the validation, however, have faint differences. The validation accuracy follows an overall increasing pattern, reaching astonishing 85.70% at the conclusion of the training, whereas the validation loss is not the same, reaching its peak at the fourth epoch. All these are indicative of the fact that the model will be learning the training data in an effective way, but the validation performance would be a little volatile or overfitted.

VGG-19 architecture of deep convolutional neural network is characterized by simplicity and depth. The convolutional and max-pooling layers are followed by three completely connected layers and have a total of 19 layers. Their fine details are captured in images that are recorded in its deep structure, and this is good in challenging visual identification. This is not the only benefit it has. However, it is also limited in the fact that it demands a lot of computational power and resources and thus is not as effective when it comes to real-time use or use in devices that have minimal processing power. Moreover, due to the massive number of parameters, VGG-19 can easily overfit to smaller datasets, and the size of the model and training data characteristics ought to be thought over. Figure 11a shows the training and validation accuracy curves of the VGG-19 model. The model obtained a high accuracy of 95% during the training process, which shows that it has a strong ability to group pictures according to their accurate classification. The accuracy in validation of 95% means that the model is able to generalize well on unknown data. Results of the training and validation loss curve of VGG-19 are presented in Figure 11b. The loss of the model is minimized in the training set of data, which points to how well the model fits. VGG-19 model has good learning and generalization capacity with its low loss of 0.15 which means that it has the ability to make accurate predictions with low error margin.
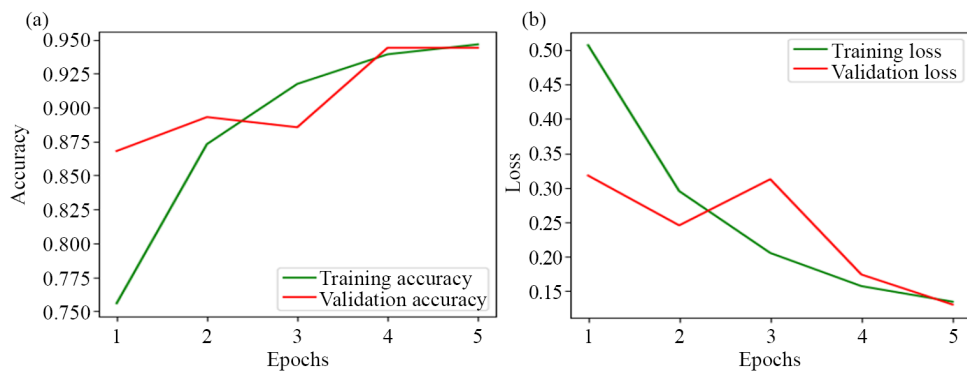

Figure 11. (a) Training and validation accuracy of VGG 19, (b) Training and validation loss of VGG 19

Table 4. Accuracy and loss of VGG-19 model on training and validation data

Epoch	Training loss	Training accuracy	Validation loss	Validation accuracy
1	0.5072	0.7559	0.3177	0.8680
2	0.2951	0.8731	0.2453	0.8930
3	0.2052	0.9174	0.3124	0.8855
4	0.1570	0.9392	0.1739	0.9440

The VGG-19 model was trained in five epochs and both the training and validation performance increased steadily. The training loss decreased by 0.5072 to 0.1344 as shown in Table 4, which shows that the model was more adjusted to the training dataset. Accuracy in training rose to 94.65% at the same period as compared to the 75.59%. The validation results were also positive with accuracy increasing to 94.40% and loss reducing to 0.1303. Such findings suggest that the VGG-

19 model was quite good at image classification, as it learnt and generalized image patterns on the dataset. Among the numerous advantages of the InceptionV3 is the fact that it is efficient to capture detailed patterns due to the employment of inception modules, which use filters with different widths. Due to the reduced number of parameters in the design, the training and inference can occur faster, making computing efficient. However, due to its structure, having many layers and modules, InceptionV3 might be hard to comprehend. Moreover, the complexity and richness of the model could lead to increased processing processes, which might limit its application in resource-oriented settings. Despite these problems, InceptionV3 remains a good choice to use when it comes to picture classification tasks, as it offers a balance between computational efficiency and accuracy.
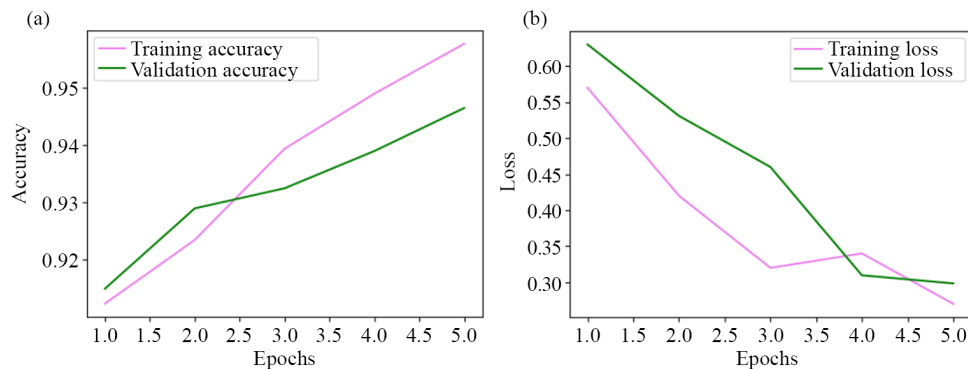

Figure 12. (a) Training and validation accuracy of Inception V3, (b) Training and validation Loss of Inception V3

The figure above is the training and validation loss of the Inception V3 model during 5 epochs, as well as its accuracy. Within the framework of the epochs, the accuracy of validation increases to 94.65% and the training accuracy to 95.77%. Loss in the training and the validation loss decreases to 0.270 and 0.2984 respectively. Accuracy and loss both have positive trends and thus, these metrics indicate that the Inception V3 model is learning effectively. Figure 12a and Figure 12b plot graphs that would represent these trends and indicate the performance of the model during training and validation.

4.4 *Performance analysis of the proposed model*

Figure 13a provides the training and validation accuracy of GHGO-PACF. With a robust validation accuracy of 97% and high accuracy of 99% during training, the model shows that it can effectively recognize patterns in the data presented. Moreover, Figure 13b demonstrates the training and validation losses of the optimizer, and they are low with the values of 0.1 and 0.01 respectively. These results suggest that the optimizer manages to minimize the discrepancy between the expected and actual values both in the training and validation steps which improves the generalization and overall performance of the model.

Table 5. Accuracy and loss of proposed GHHO-PACF model on training and validation data

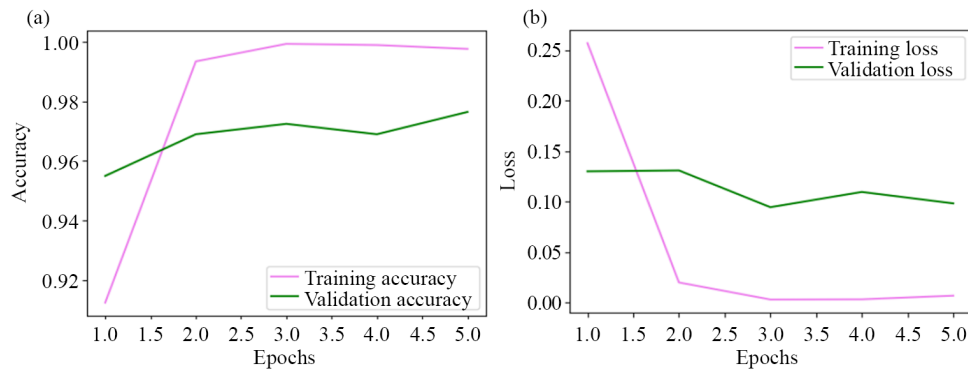| Epoch	Training loss	Training accuracy	Validation loss	Validation accuracy
1	0.2570	0.9124	0.1301	0.9550
2	0.0201	0.9935	0.1310	0.9690
3	0.0032	0.9994	0.0946	0.9725
4	0.0034	0.9990	0.1097	0.9690
5	0.0070	0.9977	0.0984	0.9765

Figure 13. (a) Training and validation accuracy of GHHO-PACF classifier, (b) Training and validation loss of GHHO-PACF classifier

The Table 5 summarizes the performance measures of a machine learning model that has been trained with 5 epochs. The training loss and accuracy values of the model are indicators of the success of the model on the training dataset, with lower loss values and higher accuracy desirable. The accuracy of validation measurements and the loss give information regarding the capability of the model to predict new untested data. The evolution of these measurements through the epochs will give some information on how well the model can learn, and how well it can work on training and validation data, as well as how well the model works on the classification tasks. This will present you with the picture of its effectiveness.

The combination of performance evaluation of the better PACF and MO-GHHO has given the model based on GHHO impressive improvements to the original model. The increased learning ability and increased generalization are provided by the optimized model training accuracy of 99.6% and validation accuracy of 98.2%. To a significant degree, such increase in performance is understood in terms of the multi-objective optimization, which MO-GHHO chooses to follow, which moderates loss throughout the training process and enhances the resistance of the model to the diversity of alterations in features distribution. These training values, validation loss values imply that such improvement is further supported and the final values obtain 0.0025 and 0.078 respectively.

The obtained results suggest a more effective convergence and an account of lesser chance of overfitting. Multi-objective formulation has the advantage of balancing the bias and variance, and it leads to a more stable and generalizable model. Also, the MO-GHHO model shows stable performance during training epochs with little variation in both the accuracy and loss levels. This performance is enhanced by the use of an adaptive meta-learning and feature-specific classifier-fusion framework, merging the PACF and integrating this in conjunction with the adaptive meta-learning and feature-based classifier fusion. In general, the suggested PACF and MO-GHHO methodology presents a reliable, correct, and flexible response to complicated pattern recognition problems. The crucial performance indicators of the PACF and MO-GHHO model over training epochs are summarized in Table 6 which highlights the ability of the model to keep low loss, and high accuracy on both training and validation sets repeatedly throughout training.

Table 6. Accuracy and loss of proposed MO-GHHO-PACF model on training and validation data

Epoch	Training loss	Training accuracy	Validation loss	Validation accuracy
1	0.1892	0.9340	0.1104	0.9615
2	0.0150	0.9958	0.0958	0.9730
3	0.0025	0.9996	0.0836	0.9795
4	0.0029	0.9993	0.0792	0.9810
5	0.0027	0.9995	0.0780	0.9820

Table 7 provides a comparison of two models, the one proposed in this case and the baseline PACF + GHHO among key performance parameters. The findings denote that the combination of both the MO-GHHO and the descendants of GHHO tends to better the original GHHO based strategy. The value of training accuracy of PACF + MO-GHHO is 99.96%, which is a little bit more than 99.94 of recognition accuracy of PACF + GHHO model. More importantly, the validation performance increases to 98.20 percent compared to 97.65 percent indicating a better generalization performance on unknown data. By the value of losses, the PACF + MO-GHHO model has a lower value of training loss (0.0025 vs. 0.0032) and validation loss (0.0780 vs. 0.0946), which proves the efficient learning and less overfitting. Moreover, the PACF + MO-GHHO model has a better convergence stability and has stayed high in performance and showed minimal oscillations during epoch and had zero changes. The Improvement column with the indication of the √ marks support the accuracy of the proposed model that it is superior to the baseline in all the measures used to test it. In sum, the table proves the conclusion that the model PACF + MO-GHHO has the better performance, better robustness and more stable convergence behavior than the traditional PACF + GHHO one.

Table 7. Comparative analysis between PACF + GHHO and PACF + MO_GHHO

Metric	PACF + MO_GHHO	PACF + GHHO	Improvement
Training accuracy	99.96%	99.94%	√
Validation accuracy	98.20%	97.65%	√
Training loss	0.0025	0.0032	√
Validation loss	0.0780	0.0946	√
Convergence stability	high	better	√

A comparison of the accuracy of the balanced and unbalanced datasets is shown in Figure 14. The performance of models trained on different types of datasets is graphically compared in a graph. The Y-axis shows the corresponding accuracy values, and the X-axis perhaps shows multiple models or experiments. The purpose of this graph is to provide insight into how the class distribution and balance of the data set affects the overall performance of the model. The performance of the model is evaluated using a comparative study considering F1 score, precision, precision, and recall. Recall evaluates the detection of positive events, precision evaluates the overall correctness, precision evaluates the accuracy of positive predictions, and F1 score determines the trade-off between recall and precision. This thorough analysis will help you determine the strengths and weaknesses of different models and approaches. The accuracy, precision, recall and F1 score of the model predicted based on the equations (21) to (24).

$$\text{Accuracy} = \frac{\text{true positive } + \text{ true negative}}{\text{total}} \tag{21}$$

$$\text{Precision} = \frac{\text{true positive}}{\text{true positive } + \text{ false positive}} \tag{22}$$

$$\text{Recall } = \frac{\text{true positive}}{\text{true positive } + \text{ false negative}} \tag{23}$$

$$\text{F1 score } = 2 \times \frac{\text{precision } \times \text{ recall}}{\text{precision } + \text{ recall}} \tag{24}$$
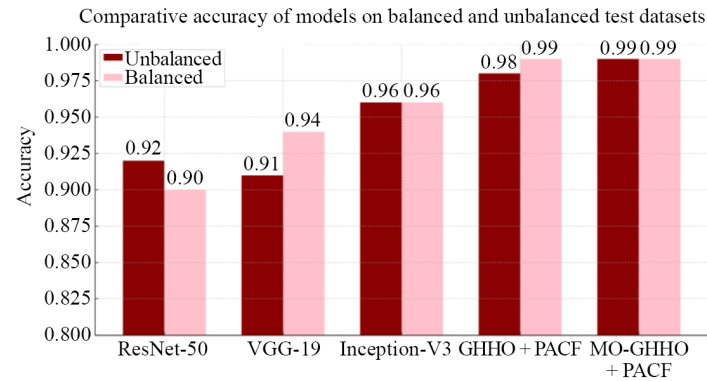
Figure 14. Comparative analysis of the accuracy of balanced and unbalanced dataset

Table 8. Comparative analysis of various state of art models

Model	Training accuracy	Testing accuracy	Training loss	Testing loss	Precision	Recall	F1 score	Training time
MO-GHHO + PACF	99.96%	98.20%	0.0023	0.07	99%	98.1%	98.5%	47
GHHO + PACF	99%	97%	0.007	0.09	98.1%	96.3%	97.2%	42
Regularized CNN	89%	87%	0.4	0.3	88.5%	85.2%	86.2%	21
ResNet-50	95%	92%	0.1	0.2	94.2%	98.1%	96.2%	37
VGG-19	94.6%	94.4%	0.134	0.13	93.3%	96.3%	94.5%	35
Inception V3	95.7%	94.6%	0.270	0.29	92.7%	94%	93%	32
MobileNet	92%	89%	0.15	0.22	91.3%	88%	89.8%	30
ResNeXt	94%	91%	0.12	0.18	93.8%	90.7%	91.3%	36
DenseNet	96%	93%	0.08	0.15	95.6%	92.1%	94.4%	39
SqueezeNet	90%	87%	0.20	0.28	88.8%	85.9%	87.4%	18
AlexNet	88%	85%	0.25	0.30	85.4%	82.7%	83.3%	27
You Only Look Once (YOLO)	96%	94%	0.10	0.18	94.5%	92.2%	93.4%	41

The Table 8 gives an apt comparative study of some of the best deep learning models in terms of key performance indications like accuracy of training and testing, loss function, precision, recall and F1 score. Such models as MO-GHHO + PACF, GHHO + PACF, Regularized CNN, ResNet-50, VGG-19, Inception V3, MobileNet, ResNeXt, DenseNet, SqueezeNet, AlexNet, and YOLO were evaluated. Out of all of the models, MO-GHHO + PACF has been the most superior, with the highest training accuracy of 99.96 percent and testing accuracy of 98.20%, and lowest training-loss as well as testing-loss of 0.0023 and 0.0756 respectively. It also provides excellent classification results with precision of 99%, recall of 98.1% and F1 score of 98.5% which shows that it is robust, stable and capable of reducing false positives and negatives. The results of the GHHO + PACF model are also good in that it has a training and testing accuracy of 99% and 97% respectively and a good F1-score 97.2%. This is the demonstration of the potential of PACF and GHHO (adaptive classification and segmentation optimization). Nevertheless, model optimization and convergence performance are increased by the introduction of MO-GHHO.

The regularized CNN has a moderate performance in both training and testing with precision of 89% and 87%, respectively, compared to the models such as the ResNet-50 and VGG-19 which have high precision with a very high percentage and generalization capacity on all aspects. The other factor about inceptionV3 is that it is highly accurate and precise with good balance in case of losses. MobileNets, ResNeXt and SqueezeNets have good loss and metrics thus can be applied where resources are limited. Meanwhile, DenseNet and YOLO demonstrate high performance in terms of the classification, in particular, the precision and recall, and can prove to be useful in satellite image analysis. Overall, the

results are a good sign that MO-GHHO + PACF hybrid model is better than the traditional and deep learning model in terms of accuracy and consistency and therefore a possible candidate of the post-disaster analysis of satellite images.

Table 9. Ablation study

Experiment	Feature subset A	Feature subset B	Feature subset C	Accuracy	Precision	Recall	F1 score
Baseline	Enabled	Enabled	Enabled	92.2%	90.3%	92.8%	91.1%
Experiment 1	Disabled	Enabled	Enabled	88.9%	86.7%	89.2%	87.5%
Experiment 2	Enabled	Disabled	Enabled	90.3%	88.9%	91.7%	89%
Experiment 3	Enabled	Enabled	Disabled	87.7%	85.4%	88.3%	86%
Experiment 4	Disabled	Disabled	Enabled	85.7%	82.8%	87%	84.7%

Table 9 presents the results of an ablation study, systematically evaluating the impact of disabling specific features on the performance metrics of a model and naming the feature subset as A, B and C. Feature subset A represents statistical measures such as mean, standard deviation, skewness of pixel intensities in different regions of the satellite images. Feature subset B represents the texture features, edge information, spectral features that are relevant for detecting specific patterns associated with hurricane impact. Feature subset C includes spatial relationships, contextual information, or any other characteristics that provide insights into the post-hurricane scenario. The Baseline configuration, with all features enabled, achieves an accuracy of 92.8%, precision of 90.3%, recall of 92.8%, and F1 score of 91.1%. Subsequent experiments involve disabling individual features, revealing their influence on the model's performance. For instance, in Experiment 1, disabling Feature A results in a slight decrease in accuracy to 88.9%, along with reductions in precision, recall, and F1 score. Similar trends are observed in other experiments, highlighting the importance of each feature in contributing to the overall effectiveness of the model. The performance of the proposed work is applied to two different dataset such as water bodies land classification as shown in Table 10.

Table 10. Performance analysis of proposed work for other datasets

Model	Dataset	Accuracy	Precision	Recall	F1 score
GHHO + PACF	Satellite images of water bodies	94.3%	93.2%	95.1%	94.1%
	Satellite image classification of land	96.8%	97.9%	96.8%	97.5%
MO-GHHO + PACF	Satellite images of water bodies	96.1%	95%	97.3%	96.7%
	Satellite image classification of land	98.2%	98.7%	98.4%	98.7%

The performance analysis of the proposed work for two different tasks on different datasets Satellite Image Classification of Land and Satellite Images of Water Bodies is shown in Table 10. The suggested model demonstrated its capacity to recognize and segment water bodies in satellite imagery with an accuracy of 94.3% for the job of satellite images of water bodies. The model's recall of 95.1% shows that it is proficient at collecting a large proportion of actual water pixels, while its precision of 93.2% indicates that it can classify pixels as water with accuracy. The harmonic mean of precision and recall is used to produce the F1 Score, which comes out at 94.1%, indicating a balanced performance in both areas. The suggested model showed a greater accuracy of 96.8% in the context of Satellite Image Classification of Land, demonstrating its efficacy in precisely classifying land features. The precision of 97.9% highlights the model's accuracy in recognizing land pixels by indicating a low false positive rate. Furthermore, the recall of 96.8% indicates that the model can accurately capture a significant proportion of real land pixels. The overall good performance is highlighted by the F1 Score of 97.5%, which confirms the proposed work's effectiveness in classifying land features from satellite images. Additionally, the MO-GHHO + PACF model is with better results in both datasets. On the dataset Satellite Images of Water Bodies, it got an 96.1% accuracy, 95% precision, 97.3 percent recall, and a F1 Score of 96.7. The model

implemented on the Satellite Image Classification of Land achieved 98.2% accuracy, 98.7% precision, 98.4% recall and F1 Score of 98.7% also confirming improved efficiency of the proposed method. Together, these findings demonstrate the suggested model's resilience and adaptability to a variety of datasets and tasks as shown in Figure 15.
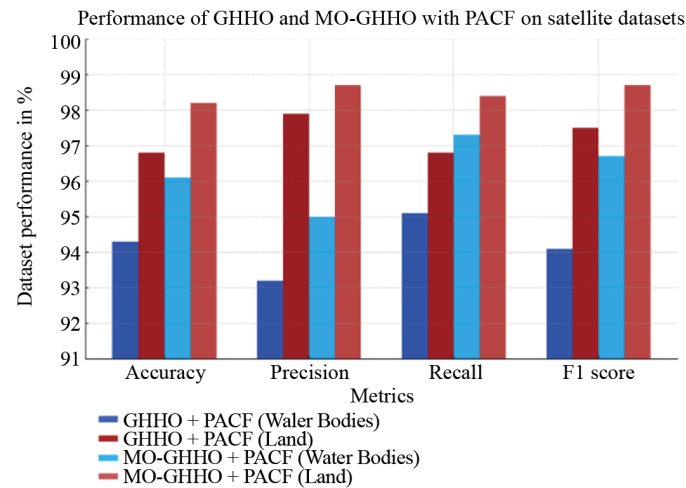

Figure 15. The performance of satellite images of water bodies and Land

Figure 15 provides a comparative analysis of two optimization models GHHO + PACF and MO-GHHO + PACF, in two types of satellite datasets. The findings indicate that MO-GHHO + PACF will over-perform GHHO + PACF in all the metrics and data sets. The most effective performance by MO-GHHO + PACF on the Land dataset is with all the metrics being close to or more than 98.5%, which is quite reliable and accurate. Conversely, the lower performance indicated with the Water Bodies dataset results in a notable upsurge of the performance occasioned by the MO-GHHO enhancement. Though it gave decent (mainly 93% to 97%) results, the GHHO + PACF model is not as good as the multi-objective version. Such comparison indicates the strength of the MO-GHHO + PACF framework in particular cases when the maximum precision and recall are paramount.

There are a number of uncertainties in the data of remote sensing including the variations in the image resolution, atmospheric noise, and cloud cover which may influence the model performance. Moreover, model parameters, such as hyperparameters and architecture choices bring sensitivity into the results, which we dealt with by systematic tuning. Weaknesses of this work are that it is based on relatively small datasets, predetermined training, validation, and testing distribution, and the computational cost of hybrid models. To further develop the model in the future, we would suggest using larger and more heterogeneous datasets, cross-validation to test the models more rigorously, more efficient computational planning, and the application of the framework to other remote sensing tasks including multi-temporal analysis or multi-sensor fusion.

5. Conclusions

There is an urgent need for quick and precise damage assessment in the field of post-hurricane satellite image analysis. Hurricanes and other natural disasters require excellent methods for assessing the level of destruction to plan prompt and efficient response plans. Deep learning models have shown to be invaluable tools for automating this difficult process. The assessed models Regularized CNN, ResNet-50, VGG-19, Inception V3, and more have demonstrated their ability to identify and classify patterns of damage in satellite data. These models are an important first step in developing scalable and trustworthy responses to large-scale disaster scenarios.

This paper suggested a new hybrid solution as the Gradient-Hopping Hybrid Optimizer with (GHHO + PACF) to overcome current drawbacks and improve accuracy. Through this framework of the segmentation optimization and adaptive classification, it can give extraordinary performance with 99% training accuracy and 97% testing accuracy. The model efficiently balances precision, recall, and F1 score thus it is very applicable in detecting hurricane induced damages in satellite images. GHHO contributes to greater optimization level, whereas PACF lets to reliably upgrade decision-making process of the classifier, leading to efficient generalization over larger, never-before-seen data. On this basis, the study also proposed the Multi-Objective GHHO integrated with PACF (MO-GHHO + PACF) that also includes multi-objective optimization to adjust segmentation parameters and enhanced convergence. In numerous datasets, this improved model surpasses GHHO + PACF in all major measures of performance, such as 96.1% accuracy in the images of satellite water bodies and 98.2% accuracy on the satellite image classification of land. The heightened level of precision and recall reinforces its achievement in additional multifarious and ramified classification tasks, thereby providing enhanced levels of scale-ability, durability, and optimization. In a summary, the new GHHO + PACF and MO-GHHO + PACF frameworks would greatly enhance post-disaster image analysis to provide high accuracy, convergence time, and accuracy in damage detection. The models present great prospect as practical tools of benefit in the context of disaster management in real world where timely action can be taken and better decision made when recovering disaster areas.

Acknowledgement

Availability of data

The datasets are available online PostHurricane Satellite Imagery Dataset https://www.kaggle.com/datasets/ravind ramanne/posthurricane/data, Satellite Images of Water Bodies https://www.kaggle.com/code/prasadmeesala/water-bodie s-segmentation/input, Satellite Image Classification of Land https://www.kaggle.com/datasets/mahmoudreda55/satellit e-image-classification.

Conflict of interest

The authors declare no competing financial interest.

References

[1] Singh DK, Hoskere V. Post disaster damage assessment using ultra-high-resolution aerial imagery with semi-supervised transformers. *Sensors*. 2023; 23(19): 8235. Available from: https://doi.org/10.3390/s23198235.

[2] Xia H, Wu J, Yao J, Zhu H, Gong A, Yang J, et al. A deep learning application for building damage assessment using ultra-high-resolution remote sensing imagery in Turkey earthquake. *International Journal of Disaster Risk Science*. 2023; 14(6): 947-962. Available from: https://doi.org/10.1007/s13753-023-00526-6.

[3] Jozi D, Shirzad-Ghaleroudkhani N, Luhadia G, Abtahi S, Gül M. Rapid post-disaster assessment of residential buildings using Unmanned Aerial Vehicles. *International Journal of Disaster Risk Reduction*. 2024; 111: 104707. Available from: https://doi.org/10.1016/j.ijdrr.2024.104707.

[4] Soleimani R, Soleimani-Babakamali MH, Meng S, Avci O, Taciroglu E. Computer vision tools for early post-disaster assessment: Enhancing generalizability. *Engineering Applications of Artificial Intelligence*. 2024; 136: 108855. Available from: https://doi.org/10.1016/j.engappai.2024.108855.

[5] Zainal N, Sithambranathan M, Khattak UF, Zain AM, Mostafa SA, Deris AM. Optimization of electrical discharge machining process by metaheuristic algorithms. *Qubahan Academic Journal*. 2024; 4(1): 277-289. Available from: https://doi.org/10.48161/qaj.v4n1a465.

[6] Shojaei B, Naserabadi HD, Amiri MJT. Optimizing competency-based human resource allocation in construction project scheduling: A multi-objective meta-heuristic approach. *Qubahan Academic Journal*. 2024; 4(3): 861-881.

[7] Arabi Aliabad F, Ghafarian Malamiri H, Sarsangi A, Sekertekin A, Ghaderpour E. Identifying and monitoring gardens in urban areas using aerial and satellite imagery. *Remote Sensing*. 2023; 15(16): 4053. Available from: https://doi.org/10.3390/rs15164053.

[8] Haghighi GE, Hanieh B, Javad VZM, Ebrahim G. Fusion of aerial and satellite images for automatic extraction of building footprint information using deep neural networks. *Information*. 2025; 16(5): 380. Available from: https://doi.org/10.3390/info16050380.

[9] Roy SK, Jamali A, Chanussot J, Ghamisi P, Ghaderpour E, Shahabi H. SimPoolFormer: A two-stream vision transformer for hyperspectral image classification. *Remote Sensing Applications: Society and Environment*. 2025; 37: 101478. Available from: https://doi.org/10.1016/j.rsase.2025.101478.

[10] Alkhatib MQ, Al-Saad M, Aburaed N, Almansoori S, Zabalza J, Marshall S, et al. Tri-CNN: A three-branch model for hyperspectral image classification. *Remote Sensing*. 2023; 15(2): 316. Available from: https://doi.org/10.3390/rs15020316.

[11] Zhao X, Ma J, Wang L, Zhang Z, Ding Y, Xiao X. A review of hyperspectral image classification based on graph neural networks. *Artificial Intelligence Review*. 2025; 58(6): 172. Available from: https://doi.org/10.1007/s10462-025-11169-y.

[12] Cao QD, Choe Y. Post-hurricane damage assessment using satellite imagery and geolocation features. *arXiv:201208624*. 2020. Available from: https://arxiv.org/abs/2012.08624.

[13] Bhardwaj D, Nagabhooshanam N, Singh A, Selvalakshmi B, Angadi S, Shargunam S, et al. Enhanced satellite imagery analysis for post-disaster building damage assessment using integrated ResNet-U-Net model. *Multimedia Tools and Applications*. 2025; 84(5): 2689-2714. Available from: https://doi.org/10.1007/s11042-024-20300-0.

[14] Ramlal B, Davis D, De Bellott K. A rapid post-hurricane building damage assessment methodology using satellite imagery. *West Indian Journal of Engineering*. 2018; 41(1): 26-35.

[15] Radhika S, Tamura Y, Matsui M. Cyclone damage detection on building structures from pre-and post-satellite images using wavelet-based pattern recognition. *Journal of Wind Engineering and Industrial Aerodynamics*. 2015; 136: 23-33. Available from: https://doi.org/10.1016/j.jweia.2014.10.018.

[16] McCarthy MJ, Jessen B, Barry MJ, Figueroa M, McIntosh J, Murray T, et al. Mapping hurricane damage: A comparative analysis of satellite monitoring methods. *International Journal of Applied Earth Observation and Geoinformation*. 2020; 91: 102134. Available from: https://doi.org/10.1016/j.jag.2020.102134.

[17] Kosianka JW, Allen MA, Rodgers N. Pre-and post-storm hurricane monitoring via data-driven SAR-based analytics. In: *Space, Satellites, and Sustainability II*. Glasgow, United Kingdom: SPIE; 2021. p.55-64.

[18] Guo J, Wu S. Damage analysis on post-hurricane images taken by satellite based on multiple variants of convolutional neural networks. In: *2021 2nd International Conference on Big Data and Artificial Intelligence and Software Engineering (ICBASE)*. Zhuhai, China: IEEE; 2021. p.515-518.

[19] Jiang S, Friedland CJ. Automatic urban debris zone extraction from post-hurricane very high-resolution satellite and aerial imagery. *Geomatics, Natural Hazards and Risk*. 2016; 7(3): 933-952. Available from: https://doi.org/10.1080/19475705.2014.1003417.

[20] Kaur S, Gupta S, Singh S, Koundal D, Zaguia A. Convolutional neural network-based hurricane damage detection using satellite images. *Soft Computing*. 2022; 26(16): 7831-7845. Available from: https://doi.org/10.1007/s00500-022-06805-6.

[21] Dotel S, Shrestha A, Bhusal A, Pathak R, Shakya A, Panday SP. Disaster assessment from satellite imagery by analysing topographical features using deep learning. In: *Proceedings of the 2020 2nd International Conference on Image, Video and Signal Processing*. New York: Association for Computing Machinery; 2020. p.86-92. Available from: https://doi.org/10.1145/3397403.3397415.

[22] Li Y, Ye S, Bartoli I. Semisupervised classification of hurricane damage from postevent aerial imagery using deep learning. *Journal of Applied Remote Sensing*. 2018; 12(4): 045008. Available from: https://doi.org/10.1117/1.JRS.12.045008.

[23] Wang W, Qu JJ, Hao X, Liu Y, Stanturf JA. Post-hurricane forest damage assessment using satellite remote sensing. *Agricultural and Forest Meteorology*. 2010; 150(1): 122-132. Available from: https://doi.org/10.1016/j.agrformet.2009.09.009.

[24] Edee K. Augmented Harris hawks optimizer with gradient-based-like optimization: Inverse design of all-dielectric meta-gratings. *Biomimetics*. 2023; 8(2): 179. Available from: https://doi.org/10.3390/biomimetics8020179.

[25] Tu B, Wang F, Huo Y, Wang X. A hybrid algorithm of grey wolf optimizer and Harris hawks optimization for solving global optimization problems with improved convergence performance. *Scientific Reports*. 2023; 13: 22909. Available from: https://doi.org/10.1038/s41598-023-49754-2.

[26] Cruz RM, Sabourin R, Cavalcanti GD. META-DES.H: A dynamic ensemble selection technique using meta-learning and a dynamic weighting approach. In: *2015 International Joint Conference on Neural Networks (IJCNN)*. Killarney, Ireland: IEEE; 2015. p.1-8.

[27] Dou P, Huang C, Han W, Hou J, Zhang Y, Gu J. Remote sensing image classification using an ensemble framework without multiple classifiers. *ISPRS Journal of Photogrammetry and Remote Sensing*. 2024; 208: 190-209. Available from: https://doi.org/10.1016/j.isprsjprs.2023.12.012.

[28] Thiagarajan K, Manapakkam Anandan M, Stateczny A, Bidare Divakarachari P, Kivudujogappa Lingappa H. Satellite image classification using a hierarchical ensemble learning and correlation coefficient-based gravitational search algorithm. *Remote Sensing*. 2021; 13(21): 4351. Available from: https://doi.org/10.3390/rs13214351.